Pis'ma v ZhETF, vol. 92, iss. 5, pp. 381 – 385

Structural, electronic properties and Fermi surface of the new non-centrosymmetric superconductors: 3.6 K $CaIrSi_3$ and 2.3 K $CaPtSi_3$

V. V. Bannikov, I. R. Shein, A. L. Ivanovskii[1)]

Institute of Solid State Chemistry, Ural Branch RAS, 620990 Ekaterinburg, Russia

Submitted 21 July 2010

First-principles FLAPW-GGA calculations were performed to investigate structural properties, electronic band structure, and Fermi surface topology of the newly discovered non-centrosymmetric superconductors: 3.6 K CaIrSi3 and 2.3 K $CaPtSi_3$. As a result, the peculiarities of the crystal structure, electronic bands, total and site-projected l-decomposed DOSs, and the shape of the Fermi surface for $CaIrSi_3$ and $CaPtSi_3$ were obtained and analyzed.

The recently discovered (2004, [1]) so-called non-centrosymmetric superconductors (NC-SCs) represent a very interesting group of rather unconventional superconducting materials based on crystals with lacking of lattice inversion center – unlike the overwhelming majority of known superconductors exhibiting inversion symmetry of their crystal structures.

Since an inherent feature of NC-SCs is mixing of spin-singlet and spin-triplet Cooper pairing channels, a wide variety of exotic superconducting properties have been predicted for such materials, see an overview in [2]. For example, some familiar NC-SCs such as $CePt_3Si$ [1], $CeRhSi_3$ [3], and UIr [4] belong to heavy fermion systems, where complex magnetic and superconducting effects may originate from strong correlations among d or f electrons, and therefore an unconventional pairing mechanism can be supposed which involves spin fluctuations.

On the other hand, direct *ab initio* calculations of the electronic structure and electron-phonon coupling in NC-SC $LaNiC_2$ [5] showed that this material belongs to conventional BCS-like electron-phonon superconductors with intermediate coupling constant $\lambda_{ep} \sim 0.5$.

Very recently, two new low-temperature NC-SCs: 3.6 K $CaIrSi_3$ and 2.3 K $CaPtSi_3$, were discovered, and some of their physical properties were examined [6]. Since these are non-magnetic and f-electron-free materials, they seem highly interesting as fine parent systems for further understanding of the pairing mechanism in NC-SCs. Thus, the first key step is basic characterization of their band structure and Fermi surface peculiarities.

In view of these circumstances, in this Letter we present a detailed *ab initio* study of the newly discovered NC-SCs: 3.6 K $CaIrSi_3$ and 2.3 K $CaPtSi_3$ focusing on their structural properties, electronic band structure, densities of states (DOSs), and the Fermi surface.

The considered ternary silicides $CaIrSi_3$ and $CaPtSi_3$ adopt a tetragonal non-centrosymmetric structure of the $BaNiSn_3$-like structural type (space group $I4mm$, No. 107), see Fig.1. As no atomic coordinates are re-

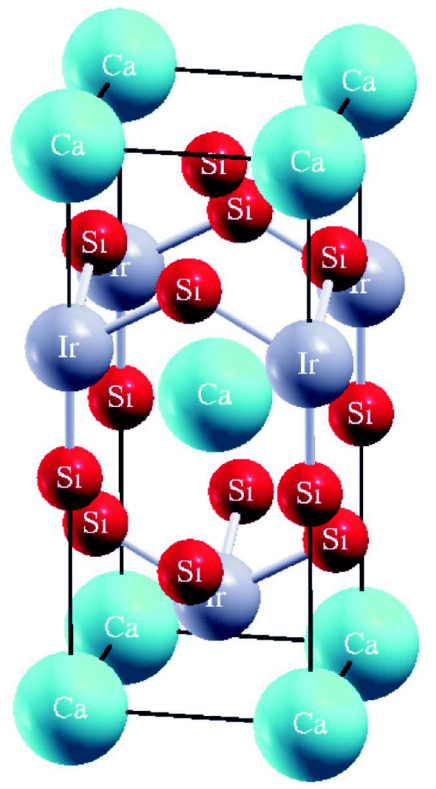

Fig.1. A fragment of the crystal structure of tetragonal (space group $I4mm$) $CaIrSi_3$ and $CaPtSi_3$. The loss of centrosymmetry is due to the arrangement of Ir(Pt) and silicon atoms

[1)] e-mail: ivanovskii@ihim.uran.ru

ported today for CaPtSi3, at the first stage the full structural optimization for $CaIrSi_3$ and $CaPtSi_3$ was performed both over the lattice parameters and the atomic positions.

Our calculations were carried out by means of the full-potential method with mixed basis APW+lo (FLAPW) implemented in the WIEN2k suite of programs [7]. The generalized gradient approximation (GGA) to exchange-correlation potential in the PBE form [8] was used. The plane-wave expansion was taken up to $R_{\mathrm{MT}} \times K_{\mathrm{MAX}}$ equal to 7, and the k sampling with $12 \times 12 \times 12$ k-points in the Brillouin zone was used. The MT sphere radii were chosen to be 2.0 a.u. for Ca, 2.3 a.u. for Ir and Pt, and 2.0 a.u. for Si. The self-consistent calculations were considered to be converged when the difference in the total energy of the crystal did not exceed 0.01 mRy and the difference in the atomic forces did not exceed 2 mRy/a.u. as calculated at consecutive steps. The hybridization effects were treated using the densities of states (DOSs), which were obtained by the modified tetrahedron method [9].

The optimized atomic positions for $CaIrSi_3$ and $CaPtSi_3$ summarized in Table 1 are in reasonable agreement with the available experiments [6]. Our data

Table 1

The optimized atomic positions and lattice constants (a and c, in) for $CaIrSi_3$ and $CaPtSi_3$

$CaIrSi_3$				$CaPtSi_3$			
atoms	x	y	z*	atoms	x	y	z
Ca	0	0	0 (0)	Ca	0	0	0
Ir	0	0	0.6416 (0.6467)	Pt	0	0	0.6420
Si(1)	0	0	0.4097 (0.4096)	Si(1)	0	0	0.4097
Si(2)	0	1/2	0.2569 (0.2589)	Si(2)	0	1/2	0.2600
a*			4.1603 (4.1833)	a			4.2232 (4.209)
c			10.1644 (9.8729)	c			10.0646 (9.816)

*Available experimental data [6] are given in parentheses.

for lattice constants (Table 1) show that *anisotropic deformation* of the crystal structure takes place when a smaller Ir atom ($R^{at} = 1.35$ Å) is replaced by a larger Pt atom ($R^{at} = 1.38$ Å),: in comparison with $CaIrSi_3$, a^{calc} for $CaPtSi_3$ increases by about $\Delta a^{\mathrm{calc}} = 0.06$ Å, whereas c^{calc} in this sequence decreases by about $\Delta c^{\mathrm{calc}} = 0.10$ Å – in reasonable agreement with experiment [6], where $\Delta a^{\mathrm{exp}} = 0.03$ Å and $\Delta c^{\mathrm{exp}} = 0.06$ Å. This *anisotropic deformation* of the crystal structure may be related to strong *anisotropy of inter-atomic bonds* (see below) – like for related layered iron-based SCs with centrosymmetric $ThCr_2Si_2$ structural type, where similar *anisotropic deformation* was also observed as a result of atomic replacements, see [10 – 15].

The band structures for $CaIrSi_3$ and $CaPtSi_3$ as calculated at equilibrium lattice parameters along the high-symmetry k lines are presented in Fig.2; the corresponding total and site-projected l-decomposed DOSs are given in Fig.3. Note that the DOS curves of the both phases have numerous van Hove singularities owing to a set of nonequivalent atoms in the unit cell complicated by various interatomic distances and by the lack of an inversion center.

The valence bands $E(k)$ for CaIrSi3 (in the range from -12.0 eV to the Fermi level $E_F = 0$ eV) can be divided into two groups. The lowest of them, located in the range from -12.0 eV to -6.3 eV (peak A, Fig.3), originate mainly from Si(1,2) s, p states with some admixture of Ir $5d$ states, and are separated by a pseudogap from the highest occupied near-Fermi bands (peaks B and C, Fig.3). In turn, these bands arise mainly from Ir $5d$ states mixed with Si(1,2) s, p states. As can be seen from atomic-resolved l-projected DOSs, Ir $5d$ states form two intense peaks located between -5.0 eV and -2.0 eV, Fig.3. Finally, in the window around E_F (peak C, Fig.3) the total DOS is formed by comparable contributions of Ir $5d$ states and Si(1,2) p states. Thus, for $CaIrSi_3$ the strong covalent Ir-Si bonding due to the overlapping of Ir $5d$ – Si(1,2) $3p$ orbitals may be supposed. Besides, it is noteworthy that the contributions from the valence states of Ca to the occupied bands of $CaIrSi_3$ (as well as for $CaPtSi_3$) are negligible, i.e. calcium atoms in these systems are in the charge states near to Ca^{2+}. This means that the Ca atomic sheets and the [Ir(Pt)-Si] blocks (see Fig.1) are linked mainly by ionic interactions.

The majority of them (with energy of 0.64 eV at Γ point) crosses E_F in directions Γ-X, Γ-P and Γ-N (Fig.1) and form complex shape of the Fermi surface (FS) with the c axis as rotation axis. In addition, one band intersects E_F in the direction X-P forming a small isolated hole-like sheet of the Fermi surface. As distinct from the above iron-based centrosymmetric $ThCr_2Si_2$-like SCs, which adopt quasi-two-dimensional cylindrical-like shapes of FSs [10 – 15], the Fermi surface for the examined NC-SC $CaIrSi_3$ adopts a complex three-dimensional multi-sheet type.

Comparison of the band structure and DOSs shapes for $CaIrSi_3$ and $CaPtSi_3$ (Figs.2 and 3) shows that for these phases the common features of their electronic spectra are kept; the obvious difference is due to an increased valence electron count ($+1\,e$) for $CaPtSi_3$ leading to the upward moving of E_F accompanied by changes in FS, Fig.4. In particular, for $CaPtSi_3$ no small isolated hole-like sheets are present, and the topology of the FS is formed by two crossed sheets (Fig.4), which

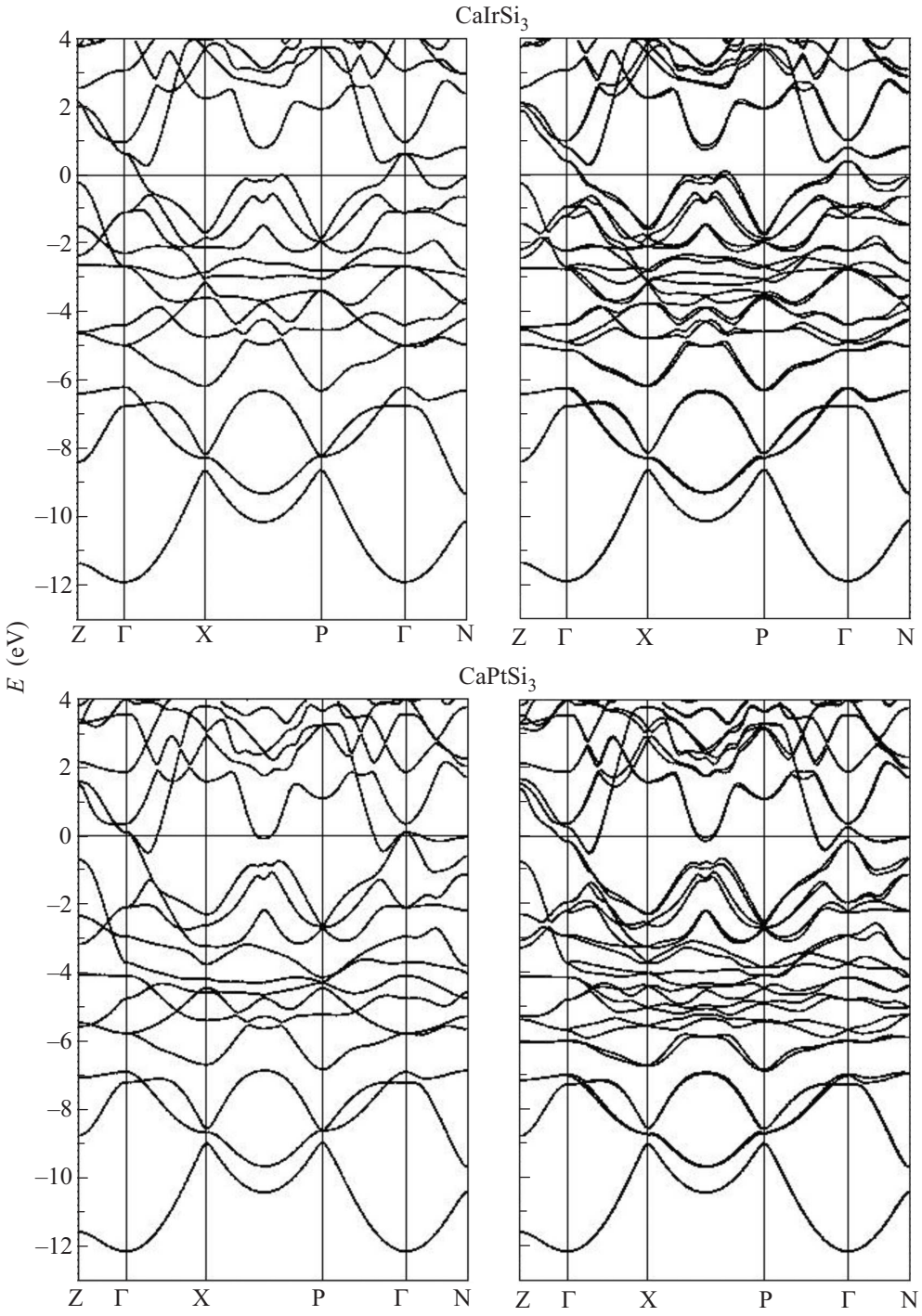

Fig.2. Electronic bands of $CaIrSi_3$ and $CaPtSi_3$. *Left panels*: non-SOC (scalar-relativistic), and *right panels*: SOC calculations

arise from the bands crossing E_F in the directions Γ-X, Γ-P, and Γ-N, Fig.2.

Some changes in the DOSs shapes for $CaIrSi_3$ *versus* $CaPtSi_3$ owing to the mentioned growth of the number of valence electrons and a more localized character of Pt $5d$ band are clearly visible in Fig.3.

Since electrons near the Fermi surface are involved in the formation of the superconducting state, it is important to figure out their nature. The total and orbital decomposed partial DOSs at the Fermi level, $N(E_F)$, shown in Table 2 allow us to make the following conclusions. For $CaIrSi_3$ the main contribution in the vicinity of the Fermi level is from Ir $5d$ states, whereas the contributions of Si(1) and Si(2) atoms are half as small. For $CaPtSi_3$, the contribution of Pt $5d$ states to $N(E_F)$ becomes much smaller; as a result, the value of

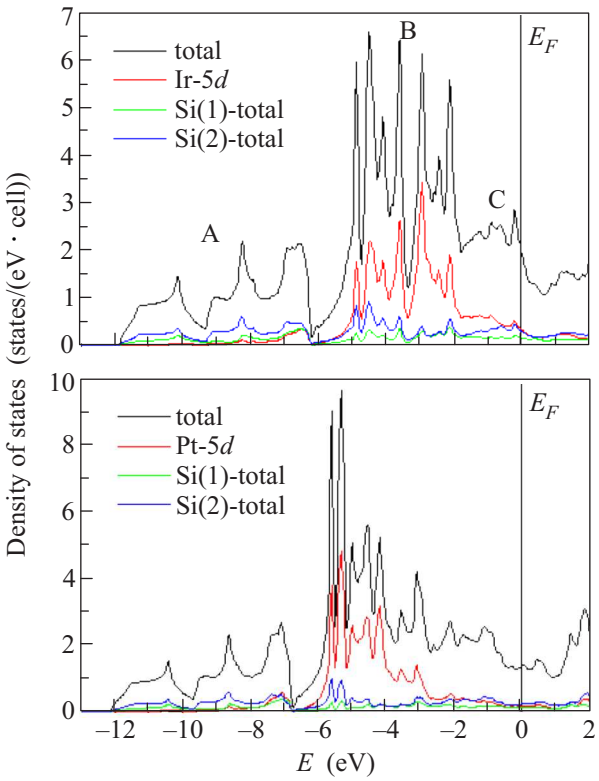

Fig.3. Total and partial densities of states of $CaIrSi_3$ and $CaPtSi_3$

Table 2

Calculated total and partial densities of states at the Fermi level for $CaIrSi_3$ and $CaPtSi_3$ compounds ($N(E_F)$, in states/eV·cell). The obtained values of Sommerfeld coefficient γ and Pauli paramagnetic susceptibility χ are also given

$N(E_F)$		$CaIrSi_3$	$CaPtSi_3$
total		1.983	1.381
Ca total		0.071	0.044
(Ir,Pt) total		0.424	0.232
	(Ir,Pt)-p	0.074	0.058
	(Ir,Pt)-d	0.332	0.168
Si(1) total		0.161	0.129
	Si(1)-s	0.017	0.008
	Si(1)-p	0.121	0.104
	Si(1)-d	0.021	0.016
Si(2) total**		0.147	0.120
	Si(2)-s	0.039	0.026
	Si(2)-p	0.090	0.080
	Si(2)-d	0.017	0.013
γ, mJ/(mol·f.u.·K^2)		4.67 (4.00)*	3.25 (2.00)
χ, 10^{-4} emu/mol		0.64	0.45

*Available experimental data [6] are given in parentheses.
**Per one atom.

$N(E_F)$ decreases as going from $CaIrSi_3$ to $CaPtSi_3$ – from 1.983 states/eV·f.u. to 1.381 states/eV·f.u.

It is well known that for low-temperature BCS-like SCs, the simplified correlations $T_c \sim N(E_F)$ are widely used for qualitative explanations of variation of T_c in the series of related materials. Thus, based on our calculations, the observed decrease in the critical temperature T_c in the sequence $CaIrSi_3$ (3.6 K)→$CaPtSi_3$ (2.3 K) [6] can be explained by reduction of $N(E_F)$. In turn, this effect is due to a decrease in the contribution of $5d$ bands to the near-Fermi region as a result of replacement of Ir atoms by platinum atoms.

The obtained data also allow us to estimate the Sommerfeld constants (γ) and the Pauli paramagnetic susceptibility (χ) for $CaIrSi_3$ and $CaPtSi_3$ under the assumption of the free electron model as $\gamma = (\pi^2/3)N(E_F)k_B^2$ and $\chi = \mu_B^2 N(E_F)$, see Table 2. The calculated γ values agree reasonably with the available experimental data [6]; both γ and χ decrease as going from $CaIrSi_3$ to $CaPtSi_3$.

Finally, the earlier discussed data are obtained using the scalar relativistic approximation, i.e. without spin-orbit coupling (non-SOC). Since the unusual effects in non-centrosymmetric superconductors are thought to originate from spin-orbit terms [1–4, 16], we examined also the influence of SOC on the electronic bands of $CaIrSi_3$ and $CaPtSi_3$. The results of our SOC calculations are presented in Fig.2. As compared with the non-SOC (scalar-relativistic) picture, the main effect in SOC calculations is the reduction of the symmetry of electronic bands and their splitting into two subbands. However, this splitting, especially in the window around E_F is small enough – no more than several meV, and the influence of SOC on $N(E_F)$ is quite negligible. So, for $CaIrSi_3$ the values of total $N(E_F)$ are 1.983 states/eV·f.u. and 2.048 states/eV·f.u. – as obtained from non-SOC (scalar-relativistic) and SOC calculations, respectively.

In summary, the first-principles FLAPW-GGA approach was used for the study of structural, electronic properties and Fermi surface topology of the newly discovered non-centrosymmetric superconductors: 3.6 K $CaIrSi_3$ and 2.3 K $CaPtSi_3$.

Our data reveal that anisotropic deformation of the crystal structure takes place if a smaller Ir atom is replaced by a larger Pt atom: the parameter a grows, whereas the parameter c decreases. This effect may be related to strong anisotropy of inter-atomic bonds, when inside [Ir(Pt)-Si] blocks strong covalent Ir(Pt)-Si bonds take place, whereas between the adjacent [Ir(Pt)-Si] blocks and Ca atomic sheets, ionic bonds emerge.

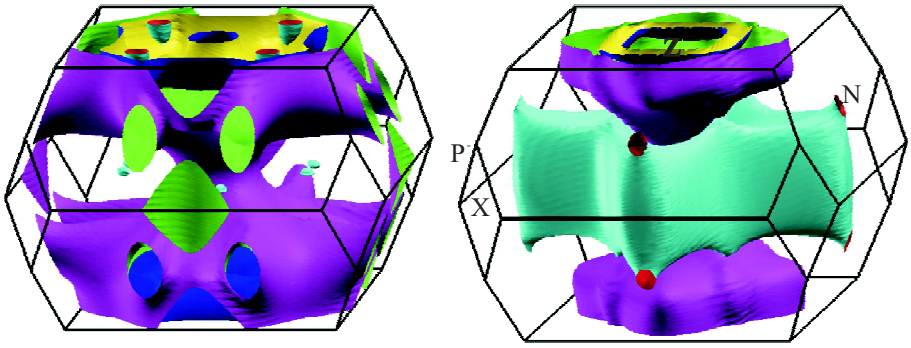

Fig.4. The Fermi surfaces of $CaIrSi_3$ (*left*) and $CaPtSi_3$ (*right*)

In general, the band structure pictures of $CaIrSi_3$ and $CaPtSi_3$ are similar, and the near-Fermi valence bands in these phases are derived from (Ir,Pt) $5d$ states with an admixture of valence Si states. We found that the effect of spin-orbit coupling for the examined phases, especially in the window around E_F, is rather small.

The main differences in the band structures and the Fermi surface topology as going from $CaIrSi_3$ to $CaPtSi_3$ are due to an increased valence electron count and a more localized nature of Pt $5d$ band. The obtained decrease in $N(E_F)$ shows that this factor can be responsible for the experimentally observed lowering of T_c in the sequence $CaIrSi_3$ (3.6 K)$\rightarrow$$CaPtSi_3$ (2.3 K) [6].

Financial support from the RFBR (Grants # 09-03-00946 and # 10-03-96008-Ural) is gratefully acknowledged.

1. E. Bauer, G. Hilscher, H. Michor et al., Phys. Rev. Lett. **92**, 027003 (2004).
2. M. Sigrist, D. F. Agterberg, P. A. Frigeri et al., J. Magn. Magn. Mater. **310**, 536 (2007).
3. N. Kimura, K. Ito, K. Saitoh et al., Phys. Rev. Lett. **95**, 247004 (2005).
4. T. Akazawa, H. Hidaka, H. Kotegawa et al., J. Phys. Soc. Jpn. **73**, 3129 (2004).
5. A. Subedi and D. J. Singh, Phys. Rev. B **80**, 092506 (2009).
6. G. Eguchi, D. C. Peets, M. Kriener et al., arXiv:1006.4807.
7. P. Blaha, K. Schwarz, G. K. H. Madsen et al., WIEN2k, *An Augmented Plane Wave Plus Local Orbitals Program for Calculating Crystal Properties*, Vienna University of Technology, Vienna, 2001.
8. J. P. Perdew, S. Burke, and M. Ernzerhof, Phys. Rev. Lett. **77**, 3865 (1996).
9. P. E. Blochl, O. Jepsen, and O. K. Anderson, Phys. Rev. B **49**, 16223 (1994).
10. A. L. Ivanovskii, Physics – Uspekhi **51**, 1229 (2008).
11. M. V. Sadovskii, Physics – Uspekhi **51**, 1201 (2008).
12. F. Ronning E. D. Bauer, T. Park et al., Physica C **469**, 396 (2009).
13. I. R. Shein and A. L. Ivanovskii, Phys. Rev. B **79**, 054510 (2009).
14. I. R. Shein and A. L. Ivanovskii, Physica C **469**, 15 (2009).
15. A. L. Ivanovskii, J. Structural Chem. **50**, 539 (2009).
16. E. Bauer, R. T. Khan, H. Michor et al., Phys. Rev. B **80**, 064504 (2009).

Pis'ma v ZhETF, vol. 92, iss. 5, pp. 386 – 389

Anisotropy of graphite optical conductivity

L. A. Falkovsky

L.D. Landau Institute for Theoretical Physics RAS, 119334 Moscow, Russia

Laboratoire de Physique des Solides, Univ. Paris-Sud, F-91405 Orsay Cedex, France

Submitted 26 July 2010

The graphite conductivity is evaluated for frequencies between 0.1 eV, the energy of the order of the electron-hole overlap, and 1.5 eV, the electron nearest hopping energy. The in-plane conductivity per single atomic sheet is close to the universal graphene conductivity $e^2/4\hbar$ and, however, contains a singularity conditioned by peculiarities of the electron dispersion. The conductivity is less in the $c-$direction by the factor of the order of 0.01 governed by electron hopping in this direction.

Recently, the light transmittance of graphene was found [1 – 3] in the wide frequency region to differ from unity by the value of $\pi\alpha$, where α is the fine structure constant of quantum electrodynamics. These experimental observations are in excellent agreement with the theoretical calculations [4, 5] of the graphene conductance, $G = e^2/4\hbar$, which does not depend on any material parameters.

This phenomenon is remarkable in two aspects. First, the fine structure constant has been found in one measurement for the first time in solid state physics. Second and most important, the Coulomb interaction does not disturb the agreement between the experiment and the theory [6, 7]. It should be emphasize that the Coulomb interaction in graphene is poorly screened while the carriers are absent in this gapless insulator.

In connection with this, it is interesting to study the change in the optical conductivity going from 2d graphene to its close "relative", 3d graphite, with the optical conductivity measured in Refs. [8, 9].

The electron properties of graphite is well described within the classical Walles-Slonczewski-Weiss-McClure theory [10]. There are many parameters in this theory of the various order of value (see, e. g. [11]). Among them, the energy $\gamma_0 = 3.1\,\text{eV}$ is largest one representing the electron in-plane hopping between nearest neighbors at the distance $r_0 = 1.42\,\text{Å}$. If we are interested in frequencies less than 3.1 eV, we can use the power $\mathbf{k}-$momentum expansion of the corresponding term in the Hamiltonian, taking only the linear approximation. Then the constant velocity $v = 10^8\,\text{cm/s}$ appears. The parameter $\gamma_1 \simeq 0.4\,\text{eV}$ known from optical studies of bilayer graphene [12, 13] is next in the order. It describes the interaction between the nearest layers at the distance $c_0 = 3.35\,\text{Å}$. The parameters γ_3 and γ_4 give corrections of the order of 10% to the velocity v. Finally, the parameters γ_2, γ_5 of the order of 0.02 eV from the third sphere are used in order to describe the dispersion of the conduction and valence bands in the $c-$direction (see Fig.1). They are usually included in order to characterize the carriers and are known from the Shubnikov-de Haas oscillations and the cyclotron resonance. However, for the optical transitions at relative high frequencies $\gamma_2, \gamma_5 \ll \omega \ll \gamma_0$, we can, first, neglect the smallest parameters γ_2, γ_5 and, second, use the linear $\mathbf{k}-$expansion with the constant velocity v for in-layer directions. Our results have the explicit analytic form.

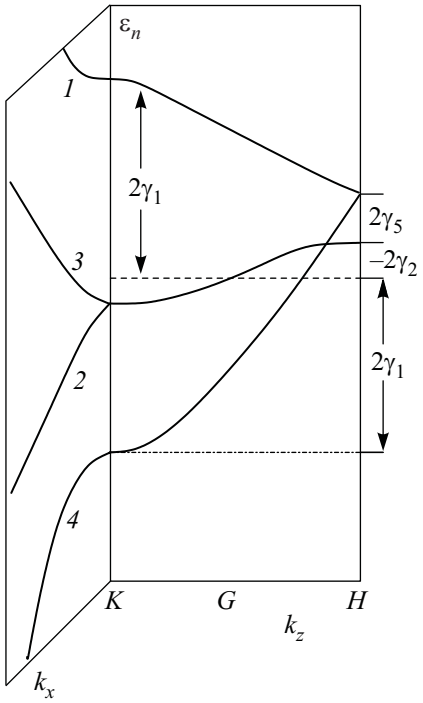

Fig.1. Dispersion of low energy bands in graphite